metals

MDPI

Article

Direct Ultrasonic Soldering of AlN Ceramics with Copper Substrate Using Zn–Al–Mg Solder

Roman Kolenak [1], Igor Kostolny [1,*], Jaromir Drapala [2], Paulina Zackova [1] and Marcel Kuruc [1]

[1] Faculty of Materials Science and Technology in Trnava, Slovak University of Technology in Bratislava, Jána Bottu č. 2781/25, 917 24 Trnava, Slovak Republic; roman.kolenak@stuba.sk (R.K.); paulina.zackova@stuba.sk (P.Z.); marcel.kuruc@stuba.sk (M.K.)

[2] FMT-Faculty of Materials Science and Technology, 17. listopadu 15, 708 33 Ostrava-Poruba, Czech Republic; jaromir.drapala@vsb.cz

* Correspondence: igor.kostolny@stuba.sk

Received: 12 December 2019; Accepted: 16 January 2020; Published: 21 January 2020

Abstract: This research aims to develop the direct soldering of aluminum nitride (AlN) ceramics with a copper substrate using Zn–Al–Mg solder. The solder type, Zn5Al3Mg, has a close-to eutectic composition with a melting point of 359 °C. The microstructure of Zn–Al–Mg solder is composed of solid solution (Al), solid solution (Zn), an Mg_2Zn_{11} phase and a minority $MgZn_2$ phase. The tensile strength is from 82 to 169 MPa and depends on the magnesium content. The bond with AlN ceramics is formed due to the interaction of active Zn, Al and Mg metals with the substrate surface without forming a new transition phase. Zn and Al elements exert a substantial effect on bond formation with the Cu substrate. Magnesium does not contribute to bond formation with the Cu substrate. Two new phases, $CuZn_4$-ε and $Cu_{33}Al_{17}/Cu_9Al_4/Cu_5Zn_8$- γ, were observed, and form the transition zone of the joint. The maximum shear strength of the AlN/Cu joint fabricated using Zn5Al3Mg solder is 47 MPa. The maximum shear strength of the Cu/Cu joint fabricated using the same solder is 93 MPa.

Keywords: ultrasonic soldering; Zn solder; boundary; active elements; shear strength

1. Introduction

The technology of soldering/brazing at higher application temperatures is considerably extended at present, and provides irreplaceable properties to the resultant products, such as excellent thermal conductivity and high reliability, and the possibility of product miniaturization [1,2].

Pb5Sn- and Pb10Sn-type high-lead solders are currently used for high-temperature applications. The greatest demand for higher application temperatures solders is shown within the electronics industry, mainly in the progressive die attach technologies. Die attach is a process of connecting a silicon chip to a substrate and/or to the support structure of a semiconductor case [3]. Progressive die attach technologies are currently in high demand, since there is great pressure exerted on electronic devices to operate faster and to be smaller, lighter and multifunctional at the same time. For this reason, many die attach technologies use high-temperature solders. These are, for example, the ball grid array (BGA), flip-chip technology (C4), chip-scale package (CSP) and/or multi-chip module (MCM) technologies [4]. Health and environmental hazards connected with the use of lead are the reason that the development of high-temperature lead-free solders have become a serious issue at present. The use of lead-free braze fillers also applies to brazing, which is confirmed by authors [5–8]. Unfortunately, in the case of soldering, there are presently only a limited number of high-temperature, lead-free alloys that would be at least partially capable of replacing high-lead solders [9].

The alternative alloy systems are, for example, hypo-eutectic Bi–Ag, Sb–Sn and Au–Sn alloys [10–12]. The other alloy systems comprise the Zn–Al solders (alloyed with Mg, Ge, Ga,

Sn and Bi), which have a promising future due to their low price. Zn–Al alloys were used for a long time as high-temperature solders for structural applications. These alloys have great potential from the commercial viewpoint, since zinc is even cheaper than Pb. Small additions of Mg and/or Ga to these alloys lower the melting point and form a ternary alloy, which preserves the desirable solidification criteria for soldering at higher application temperatures [1,13]. Zn–Al based alloys for the electronics industry have a suitable melting range, good electrical and thermal conductivity, and an acceptable price. They were, therefore, chosen by the authors [14] as a basis for their alloy. They also added Mg and Ga, resulting in Zn4Al3Mg3Ga. Copper and silicon metallized with a Ti/Ni/Ag layer were used as the substrates. Soldering was performed at 370–400 °C in automatic equipment used for die attach technology. The ZnAlMgGa/Cu joints attained a shear strength from 21.8 to 29.4 MPa at soldering temperatures of 370–400 °C, which is a value comparable to the strength of Pb5Sn/Cu joints, namely 28.2 MPa [14].

Rettenmayr et al. [15] oriented to four alternative alloys (Zn6Al, Zn6Al1Ga, Zn3Al3Mg and Zn4Al3Ga3Mg) that could substitute for classical, high-lead alloys, and they studied their microstructure and mechanical properties. They found that the temperature dependence of Ga solubility in the hexagonal lattice (hcp) of zinc, in combination with Ga affinity with the surface of phases rich in Al and Zn, is the main reason for solder brittleness. This brittleness may be reduced by lowering the solubility at higher temperatures.

The addition of Sn to the Zn4Al3Mg alloy resulted in a tensile strength increase. Zn content was added to the alloy at 0, 6, 8 and 13.2 wt %. Sn addition also resulted in reduced yield point and solidus temperature [16]. A similar solution, and addition of Sn, In and Ga elements to Zn4Al3Mg and Zn6Al5Ge alloys, was selected by Shmizu et al. [17]. Similar to the previous case, no improvement in properties was observed.

Directly soldering SiC ceramics with ultrasound assistance was studied by Chen et al. [18]. The SiC ceramic substrates were soldered in air using Zn8.5Al1Mg solder at 420 °C. The joint shear strength increased with prolonged ultrasound activation time. The highest strength (148.1 MPa) was achieved with ultrasound assistance for 8 s. A new amorphous layer, from 2 to 6 nm thick, was formed on the solder/substrate boundary. The atoms of the eroded SiO_2 layer from the SiC substrate surface diffuse quickly to the solder due to the jet effect generated by the ultrasound. The strong bond between SiC substrate and the Zn–Al–Mg solder is attributed to the transfer of SiO_2 mass to the Zn–Al–Mg solder by induced cavitation erosion.

Directly soldering sapphire (a crystalline form of Al_2O_3) with ultrasound and an application of Sn10Zn2Al solder was the subject of study of Cui et al. [19]. The ultrasound supported the oxidation reaction between Al from the solder and sapphire substrate. A nanocrystalline α-Al_2O_3 (layer 2 nm in thickness) was formed on the Sn–Zn–Al/sapphire boundary during soldering in the air at 230 °C. This layer enabled bond formation.

Cui et al. [20] also dealt with soldering sapphire using ultrasound assistance. Soldering was performed using Zn4Al solder. To lower the thermal expansivity coefficient of solder in the soldered joint, a composite SiCp/A356 interlayer was applied. The interlayer improved the shear strength of joints, even up to ~155 MPa, which represents an increase of ~250% compared to a joint where Zn–Al soldering alloy was used. The fracture morphology shows a strong bond between the Zn–Al alloy and sapphire with a mixed fracture mechanism shown in the shear test.

The aims of the presented research comprised analyzing soldering alloy type Zn5Al–Mg. The Zn, Al and Mg elements in the solder were selected because all three of them are active elements with a strong chemical affinity to oxygen. The preferred composition is Zn5Al3Mg. The composition of ZnAl5Mg3 solder corresponds approximately to a eutectic point [21]. In the point of eutectic transformation, it is valid that the solder transfers from the solid state immediately to a liquid state. However, if the solder would not be eutectic or close-to-eutectic, it would occur in the two-phase region with a certain proportion of solid phase. Thus, it would not exert sufficient viscosity [21].

The compositions were selected to be suitable for soldering the AlN ceramics and copper substrate at the defined conditions. To improve the wettability of ceramic material with Zn–Al–Mg solder, soldering with ultrasound assistance was employed. The research thus consisted of the study of solder proper and the interactions at the solder/substrate boundary.

2. Experimental

The preparation of experimental Zn–Al–Mg-Based soldering alloys consisted of a determination of weight proportions of individual weighing components and the proper manufacture of solder in an as-cast condition. The individual weighed components were of 4N purity in the form of zinc granules, 10 mm in diameter and 3 mm in thickness, and the aluminum granules 6 mm in diameter and 8 mm in thickness. Solder fabrication was realized in a vacuum oven. The procedure was as follows. Weighted amounts of alloy components were loaded into a graphite load with a 50 mm diameter siliceous glass tube. The tube was inserted into a horizontal vacuum resistance oven, so that the boat was in the heated zone. If needed, the tube could be washed with Ar, thanks to an inlet flange at its beginning and an outlet at its end. Due to significant evaporation, it was more suitable to prepare the filler metal in Ar. Magnesium was supplied in solid state in the form of pellets. It is delivered in shielding atmosphere. After taking out from the package it was wrapped with a zinc foil, and in such a combination it was dipped to a zinc melt with the temperature of 800 °C. Several metals have good solubility in the base matrix. The dissolving and homogenization of filler alloy components lasted approximately 1 h, while the melt was freely cooled down under Ar shielding. Solder alloy was remelted in a graphite crucible, thoroughly stirred and cast into a graphite mold. The soldering alloys were manufactured in the as-cast condition in the form of plates in dimensions of 100 mm × 40 mm × 4 mm.

The experimentally prepared composition of soldering alloys is given in Table 1. The chemical analysis of alloys was performed using atomic emission spectrometry with induction coupled plasma (ICP-AES). The analysis was performed on a SPECTRO VISION EOP. The alloy samples ICP-AES analysis were dissolved in suitable acid and base solutions. The analysis proper was performed on an emission atomic spectrometer with a pneumatic atomizer and Scott's atomizing chamber.

Table 1. Composition of Zn–Al and Zn–Al–Mg alloys and the results of chemical analysis by atomic emission spectrometry with induction coupled plasma (ICP-AES) [wt %].

Sample	Charge [wt %]			ICP-AES [wt %]		
	Zn	Al	Mg	Zn	Al	Mg
Zn1Al	99	1	-	99.07	0.93 ± 0.05	-
Zn2Al	98	2	-	97.97	2.03 ± 0.13	-
Zn3Al	97	3	-	97.12	2.88 ± 0.14	-
Zn4Al	96	4	-	95.99	4.01 ± 0.21	-
Zn5Al	95	5	-	94.89	5.11 ± 0.19	-
Zn5Al1Mg	94.0	5.0	1.0	94.26	4.71 ± 0.24	1.03 ± 0.06
Zn5Al2Mg	93.0	5.0	2.0	92.84	5.13 ± 0.26	2.03 ± 0.11
Zn5Al3Mg	92.0	5.0	3.0	91.98	5.07 ± 0.21	2.95 ± 0.18

Test pieces for the tensile test were subsequently prepared from these alloys (Figure 1). The dimensions given in Figure 1 are in mm. The pieces for tensile tests were prepared by water beam cutting from the cast plates in dimensions of 100 mm × 40 mm × 4 mm.

Substrates of the following materials were used in experiments:

- AlN ceramic substrate from Flocculus Ltd. (Libina, Czech Republic) in the form of discs Ø 15 × 3 mm. The purity of this AlN substrate was 3 N, and it exerted a hexagonal crystalline structure of wurtzite type.
- Al_2O_3 ceramic substrate from the Flocculus Ltd. (Libina, Czech Republic) in the form of discs Ø 15 mm × 3 mm with 3N purity,

- SiC ceramic substrate (namely SiSiC-infiltrated silicon carbide) from the CeramTec Ltd. (Šumperk, Czech Republic) in the form of discs Ø 15 mm × 3 mm,
- 4N purity metallic Cu substrate in the shape of discs with dimensions Ø 15 mm × 2 mm and in the shape of square in dimension 10 mm × 10 mm × 3 mm.

The soldered joint scheme is shown in Figure 2.

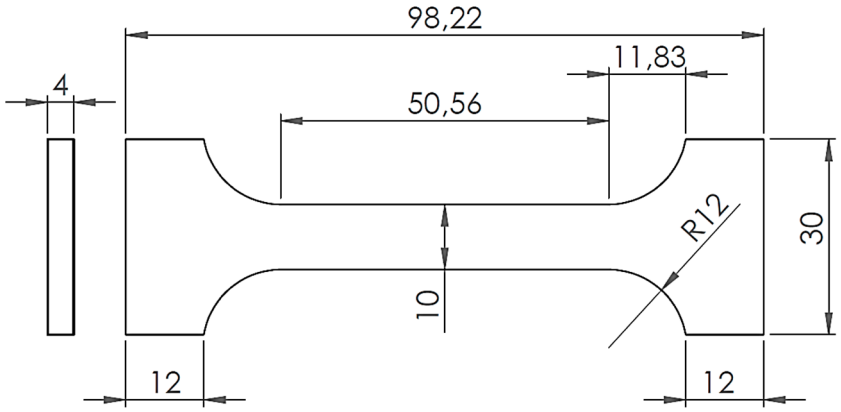

Figure 1. Test piece of solder for static tensile test. Unit: mm.

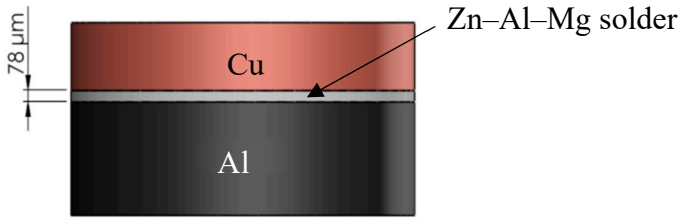

Figure 2. The fit-up of soldered joints.

Solder joints Cu/Cu, AlN/Cu, SiC/Cu and Al_2O_3/Cu were fabricated using the hot plate. The temperature was controlled with the thermostatic heat control regulator. The AlN ceramic was laid on this hot plate and filler metal in the form of a cube in the dimension of 4 mm × 4 mm, heated to soldering temperature, was deposited onto it. A flux-less soldering process using Hanuz UT2 type ultrasonic equipment was performed. The parameters of the soldering process are given in Table 2. Filler metal was activated via an ultrasonic transducer with a piezoelectric oscillating system and a titanium sonotrode with a Ø 3 mm end tip. Sufficient viscosity of solder occurs in the case, when the solder does not contain any proportion of solid phase. In accordance with the STN 050,040 Standard—Soldering and brazing. Soldering and brazing of metals. Basic terms—The optimum level of soldering temperature varies approximately from 20 to 50 °C above the liquidus temperature of the solder. The melting point of the solder was 354 to 356 °C. The temperature of soldering was measured by a NiCr/NiSi thermocouple. The ultrasonic power acting time was 5 s. The oxide layer on the surface of the liquid filler metal was then removed. A similar procedure was realized with Cu substrate. Subsequently, both substrates with liquid filler were put onto each other, and thus, the solder joint was created. This process is illustrated in Figure 3.

Metallographic preparation of specimens from soldered joints was realized by standard metallographic procedures used for specimen preparation. Grinding was performed using SiC emery papers with 240, 320 and 1200 grains/cm^2 granularity. Polishing was performed with diamond suspensions with 9, 6 and 3 µm grain sizes. The final polishing was performed using a type OP-S (Struers) polishing emulsion with 0.2 µm granularity.

Table 2. Soldering parameters.

Ultrasound Power	400	[W]
Working frequency	40	[kHz]
Amplitude	2	[μm]
Soldering temperature	370	[°C]
Time of ultrasound activation	5	[s]

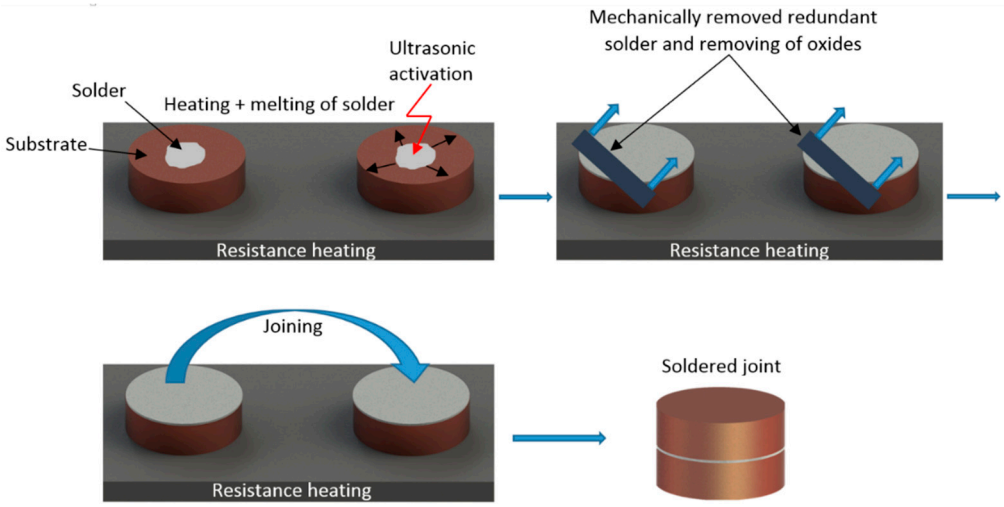

Figure 3. Schematic representation of the soldering process with ultrasound assistance.

The solder microstructure was studied using scanning electron microscopy (SEM) on TESCAN VEGA 3 (Tescan orsay holding, Brno, Czech Republic) and JEOL 7600 F (JEOL Ltd., Tokyo, Japan) with X-ray micro-analyzer type Microspec WDX-3PC microscopes (Microspec Corporation, Peterborough, NH, USA) for performing qualitative and semi-quantitative chemical analyses.

X-ray diffraction (XRD) analysis was performed to identify the solder phase composition. This analysis was done on a 10 × 10 mm solder sample using a PANalytical X'Pert PRO XRD diffractometer (Malvern Panalytical LtD., Malvern, UK).

The differential scanning calorimetry (DSC) analysis was performed on a Setaram SETSYS 18TM with a DSC sensor type E (SETARAM Instrumentation LtD., Caluire, France). The alloy specimen analyses were performed in corundum crucibles with lids in an inert Ar atmosphere (6 N). The heating and cooling rate was 5 °C/min. The weight of analyzed specimens was 100–120 mg. The specimens were ground and cleaned in acetone with simultaneous ultrasound action prior to analysis. Prior to analysis, the inner oven space was washed with Ar (6 N). The space around the specimen was vacuum pumped and then filled with Ar, while a constant dynamic atmosphere of Ar (6 N, 2 l/h) was maintained around the specimen during the entire analysis.

Shear tests were subsequently performed for determining mechanical properties.

A schematic representation of a shear test specimen is shown in Figure 4. The shear strength was determined on a versatile tearing machine, LabTest 5.250SP1-VM (Labortech Ltd., Praque, Czech Republic). For changing the direction of the loading force acting upon the test specimen, a jig with a defined test specimen shape was used (Figure 5). This shearing jig ensures a uniform shear loading in the solder/substrate boundary plane.

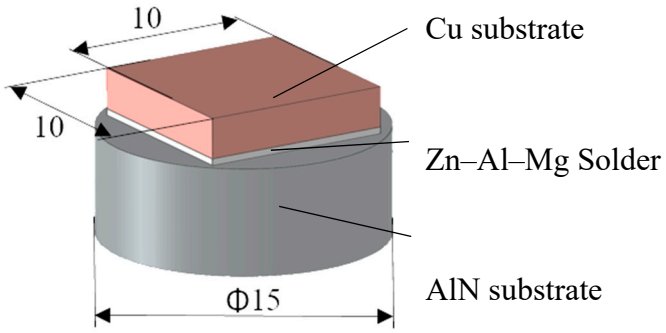

Figure 4. Specimen for shear testing the Cu/Zn–Al–Mg/AlN joint. Unit: mm.

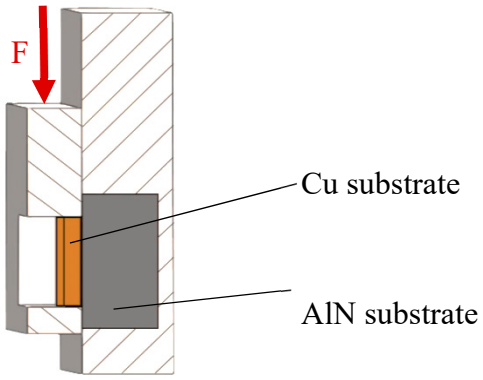

Figure 5. Scheme of shear strength measurement.

3. Experimental Results

3.1. DSC Analysis

Measurements were performed with two specimens. Four thermal effects were observed on both specimens. One effect is obvious at lowered temperature, whereas the remaining three are mutually overlapped at higher temperatures (one triple peak). Table 3 gives the significant temperatures TL, T1, T2 and T3 for the Zn5Al3Mg alloy related to thermal effects at a heating rate of 5 °C/min. The TL value is the liquidus temperature. T1 is the temperature of segregation of the Mg_2Zn_{11} phase from the melt. The T2 value is the temperature of eutectic transformation and T3 is the temperature of eutectoid transformation.

Table 3. Temperatures of phase transformations by DSC analysis.

Alloy	Heating [°C]			
	TL	T1	T2	T3
Zn5Al3Mg	356 354	348 346	340 339	275 275

Figure 6 shows a record from DSC analysis also marking significant temperatures when the phase transformations occurred in the Zn–Al–Mg system for a given alloy composition.

From the isopletic cross-section in Figure 7, valid for 3 wt % Mg, the sequence of phase formation during cooling down from the melt is as follows:

$$L \overset{359^{\circ}C}{\rightarrow} L + (Al'') \overset{350^{\circ}C}{\rightarrow} L + (Al'') + Mg_2Zn_{11} \overset{340^{\circ}C}{\rightarrow} (Al'') + Mg_2Zn_{11} + (Zn) \overset{276^{\circ}C}{\rightarrow} (Al) + Mg_2Zn_{11} + (Zn) \quad (1)$$

In comparison to the results from DSC analysis given in Table 3, the probable formation of phases agrees with relation (1).

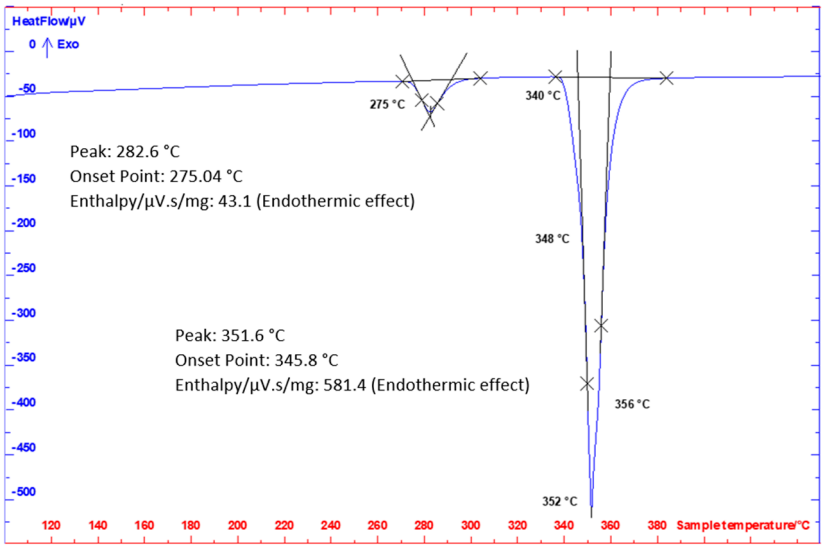

Figure 6. The differential scanning calorimetry (DSC) record for Zn5Al3Mg alloy, heating rate 5 °C/min.

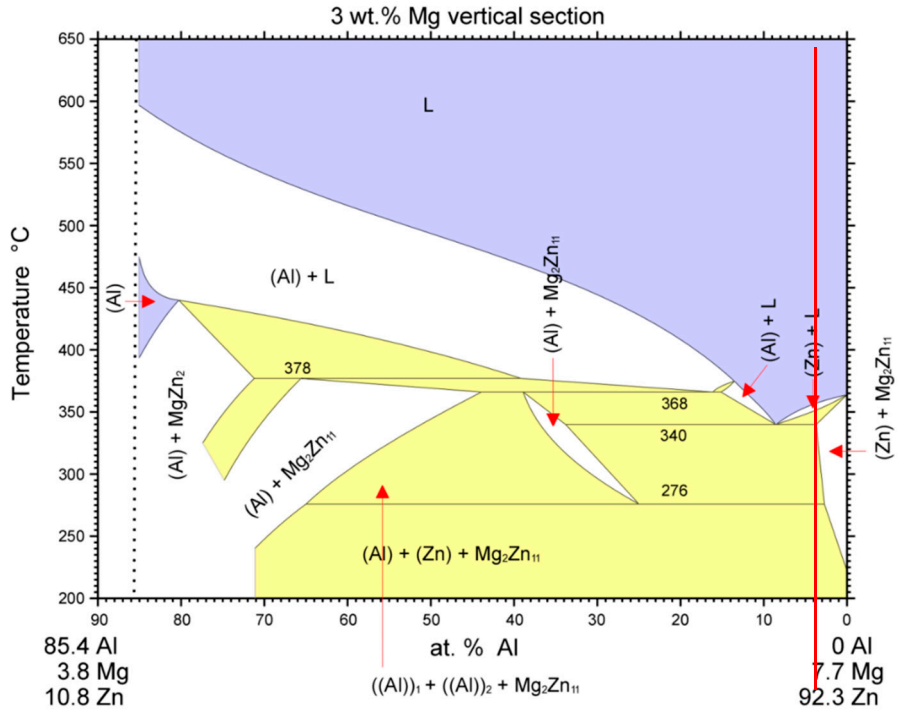

Figure 7. Isopletic cross-section through the ternary system of Al–Mg–Zn for 3 wt % Mg [22]. The red line shows the concentration of Zn5Al3Mg solder.

3.2. *Microstructure of Zn–Al–Mg Solders*

For microstructure observation, scanning electron microscopy (SEM) was employed in backscattered electron (BSE) study mode. In this BSE mode, the measure of darkening is indirectly proportional to the average atomic mass of elements present at the given point (lighter elements are shown darker—Solid solution (Al) and Mg-Zn phase; the heavier elements are shown brighter—Solid solution (Zn)).

The microstructure of Zn–Al–Mg solder is shown in Figure 8a. The solder structure consists of fine ternary eutectics, where two chemically different phases as some islands with dissimilar morphology occur. The first darker phase may be in detail seen in Figure 8b. The lamellar form of the next eutectic phase is obvious from the figure. From the stoichiometric composition, this eutectic phase is formed of

(Al“) and, from the Al–Zn phase diagram (Figure 9), it was formed between 381 and 277 °C. The second, less visible, brighter phase in Figure 8a is formed of magnesium phases.

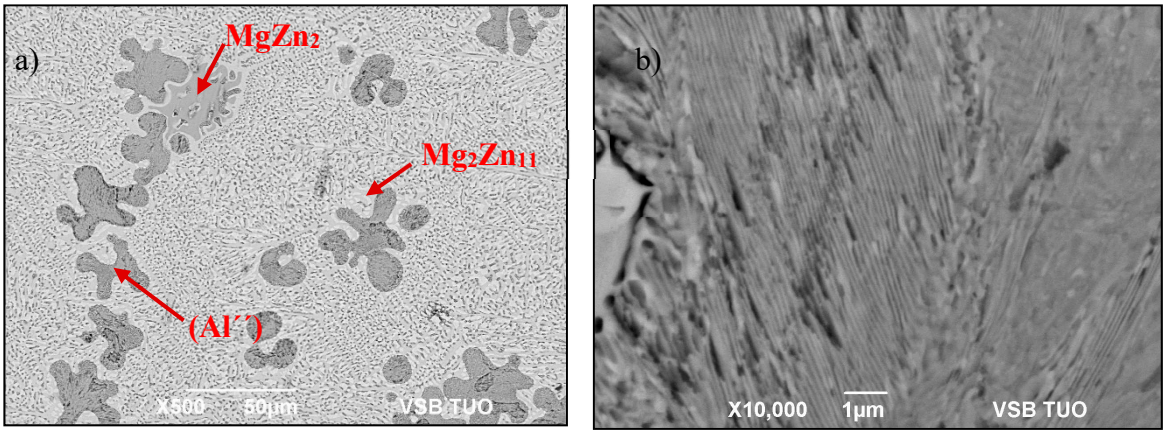

Figure 8. The Zn5Al3Mg solder (**a**) microstructure, (**b**) detailed view of darker phase (Al“).

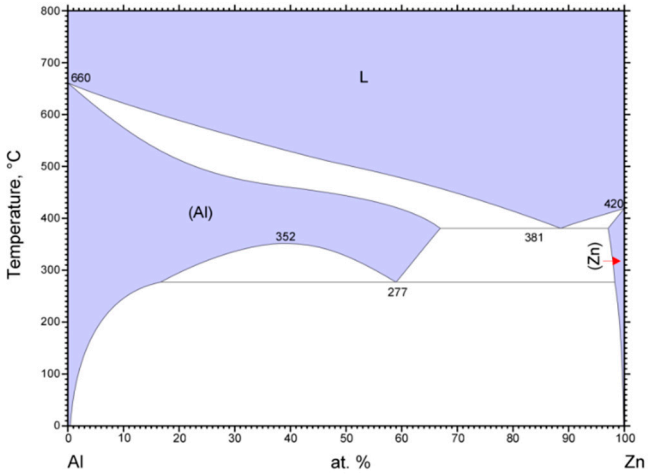

Figure 9. Phase diagram of Zn–Al [22].

To determine the chemical composition in the individual components of soldering alloy, local chemical energy-dispersive X-ray spectroscopy (EDX) microanalysis was performed. Figure 10 shows the spots where the analysis was performed, as marked with numerals; the phase composition results are given in the Table 4 below the figure. Spectrum 1 is unambiguously the $MgZn_2$ phase, where around 2.0 wt % Al is dissolved. Spectrum 2 is formed of the (Al“) phase. Spectrum 3 corresponds to the Mg_2Zn_{11} phase, which contains around 1.7 wt % Al. Spectrum 4 (eutectics) is formed of Zn and Al with high zinc content.

The XRD analysis of Zn5Al3Mg solder has proven the presence of solid solution (Zn), solid solution (Al) and an Mg_2Zn_{11} intermetallic phase. The $MgZn_2$ intermetallic phase occurs scarcely in the matrix, and it was not identified by XRD analysis. The record from diffraction analysis is shown in Figure 11.

Figure 12 shows the planar EDX analysis of Zn5Al3Mg solder, where the solder elements, Zn, Al and Mg, are distinguished in color. The islands of solid solution (Al) are clearly visible, and the space between the grains is filled with solid solution (Zn) and magnesium phase.

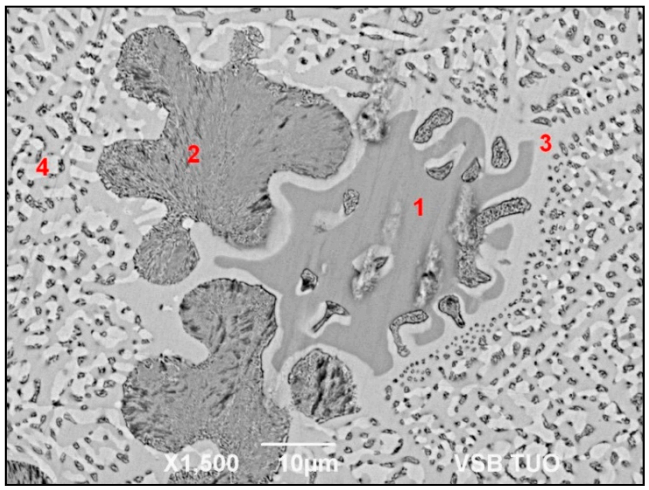

Figure 10. The energy-dispersive X-ray spectroscopy (EDX) analysis of Zn5Al3Mg soldering alloy.

Table 4. The phase composition results of Zn5Al3Mg solder alloy.

Spectrum	Zn [wt %]	Al [wt %]	Mg [wt %]	Solder Component
Spectrum 1	82.022	2.014	15.964	$MgZn_2$ phase
Spectrum 1	81.623	1.957	16.420	$MgZn_2$ phase
Spectrum 2	78.405	21.595	0	(Al“) phase
Spectrum 2	76.335	23.645	0	(Al“) phase
Spectrum 3	90.836	1.744	7.420	Mg_2Zn_{11} phase
Spectrum 3	91.515	1.756	6.728	Mg_2Zn_{11} phase
Spectrum 4	96.941	3.059	0	Zn–Al eutectic
Spectrum 4	98.235	1.765	0	Zn–Al eutectic

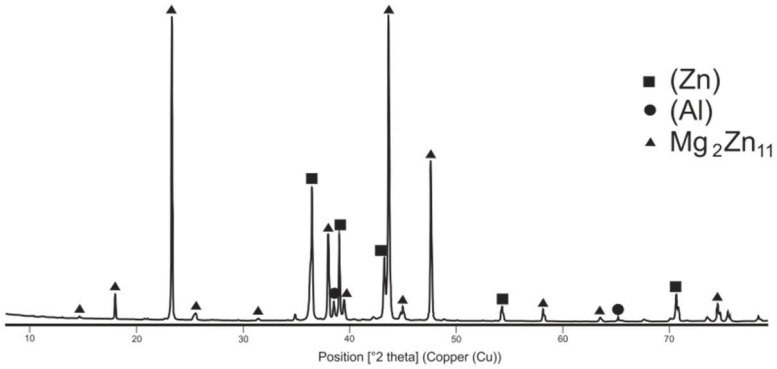

Figure 11. The diffraction record of Zn5Al3Mg solder.

3.3. Tensile Strength of Zn–Al–Mg Soldering Alloys

The mechanical tests were performed on Zn–Al–Mg solders. The test piece dimensions were proposed and calculated. Three specimens of each experimental soldering alloy were used for tensile strength measurements. The loading rate was 1 mm × min^{-1}. The tensile strength of Zn–Al–Mg solders was studied in dependence upon magnesium content. The tensile test results are documented on the graph in Figure 13.

For comparison, Figure 13 shows the tensile strength dependence of Zn–Al soldering alloys on the Al content in solder. It is obvious that with increasing Al content, the strength of the soldering alloy also increases. The highest tensile strength of 205 MPa was achieved with Zn5Al solder, which is

the principal base of Zn5Al–Mg solders. In contrast, with the addition of Mg, the tensile strength decreases. The average tensile strength value of Zn5Al1Mg solder is 169 MPa.

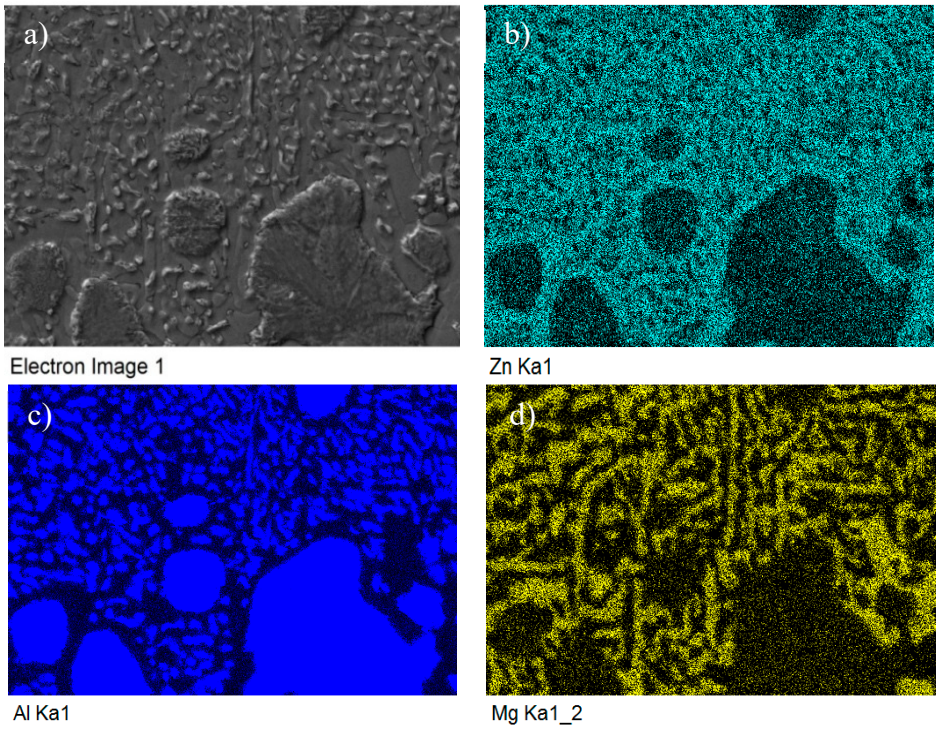

Figure 12. The map of Mg, Zn and Al elements in the structure of Zn5Al3Mg solder.

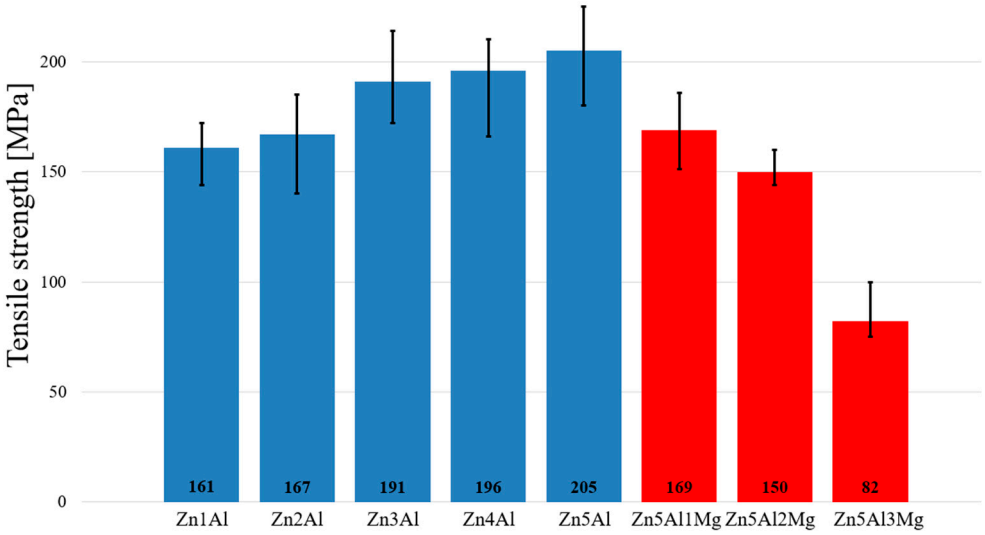

Figure 13. Tensile strength of Zn–Al–Mg soldering alloys depending on Al and Mg content.

The lowest tensile strength was observed with the highest magnesium content. The average tensile strength of Zn5Al3Mg solder is 82 MPa. These facts suggest that the addition of 2 wt % Mg decreases the tensile strength of Zn–Al–Mg solders by half. This is caused by the formation of the Mg_2Zn_{11} phase; the semiquantitative analysis revealed up to a 60% composition of that phase in Zn5Al3Mg solder.

3.4. Microstructure of AlN/Zn-Al-Mg/Cu Joint

Fabrication of an AlN/Zn-Al-Mg/Cu soldered joint was performed at 370 °C. The AlN/Zn–Al–Mg bond boundary is shown in Figure 14. It is obvious that the structure remained dendritic after soldering. The EDX analysis of the boundary is documented in Figure 15. The measurement was performed at six points, marked as Spectrum 1 to Spectrum 6 and the phase compositions are given in the Table 5 below the figure.

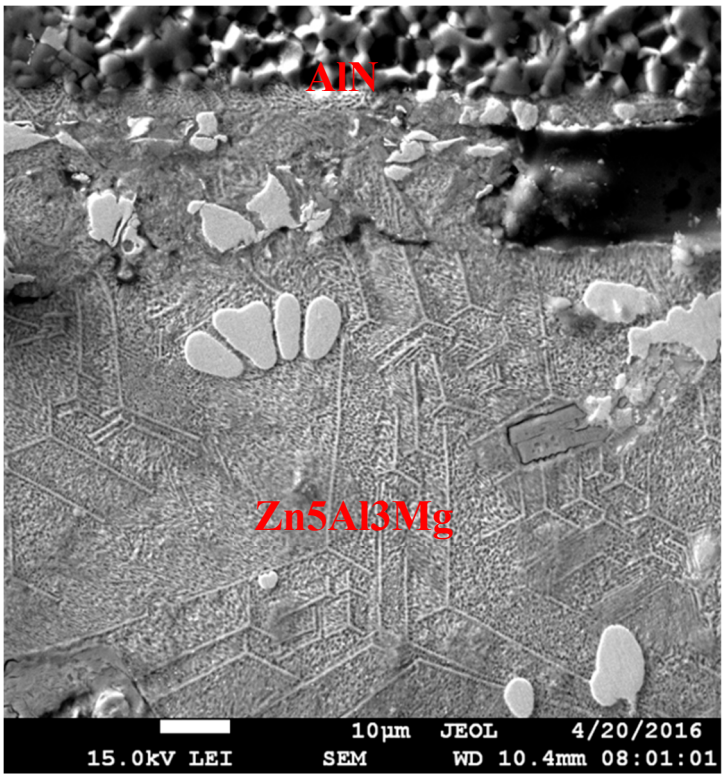

Figure 14. Microstructure of the AlN/Zn5Al3Mg boundary.

Table 5. The phase composition results of AlN/Zn-Al-Mg joint boundary.

Spectrum	Zn [wt.%]	Al [wt.%]	Mg [wt.%]	Cu [wt.%]	Component
Spectrum 1	55.43	29.35	6.76	8.45	Solder matrix
Spectrum 2	47.11	39.42	7.18	6.29	-
Spectrum 3	78.68	1.94	16.16	3.22	$MgZn_2$ phase
Spectrum 4	49.52	36.12	9.35	5.01	Solder matrix
Spectrum 5	80.68	0.90	0	18.42	$CuZn_4$-ε phase
Spectrum 6	2.11	93.38	0.29	4.22	AlN ceramics

The copper diffused from the metal substrate across the entire joint boundary. Cu presence was identified in all measurement points from Spectrum 1 to Spectrum 6. The most copper was observed in the bright phases—Spectrum 5. These bright islands are formed of $CuZn_4$-ε phase with approximately 0.9 wt.% Al. Spectrum 1 and Spectrum 4 correspond to the matrix composition with 5 to 8 wt.% Cu dissolved. Spectrum 3 corresponds to the $MgZn_2$ phase with 1.94 wt.% Al and 3.22 wt.% Cu. Spectrum 6 is situated in the zone of AlN ceramics. Small amounts of Mg, Cu and Al elements were observed.

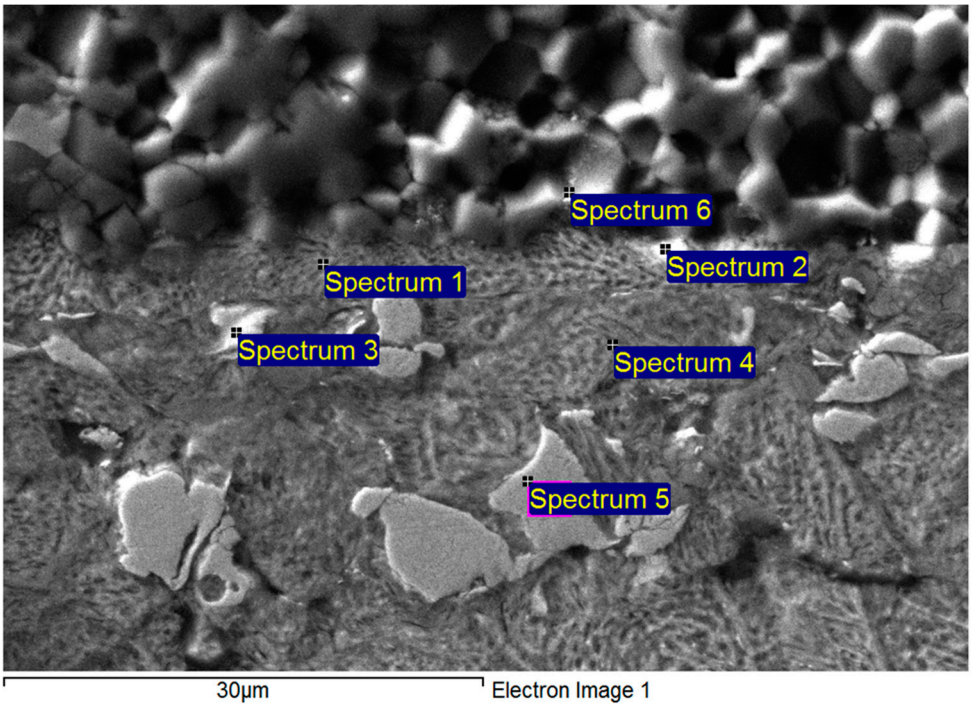

Figure 15. The EDX analysis of the AlN/Zn–Al–Mg joint boundary (marked AlN ceramics).

All active elements, Al, Zn and Mg—Spectrum 1 and 2, have similarly contributed to bond formation between AlN ceramics and Zn–Al–Mg solder. No distinct reaction layer was formed on the AlN/Zn–Al–Mg boundary. The mechanism of joint formation is as follows: The bond is formed due to interaction of Zn, Al and Mg with the surface of ceramic AlN material in the following manner: The Zn, Al and Mg particles are distributed to the boundary with AlN ceramics due to ultrasonic activation, where they are further combined with Al and N elements. The bond of these elements with AlN ceramics is of adhesive character without formation of new contact phases. Similar reaction was not observed in our study due to relatively low temperature. The mechanism of bond formation is of adhesive character. In the work [22] there was observed a thermal decomposition of AlN due to interaction of AlN ceramics with Ti-Al-Nb, where the active Ti reacted with AlN ceramics at formation of a TiN reaction product. This thermal decomposition has occurred at the temperature of 1670 °C. In our case we used the temperature of 370 °C only and therefore a similar decomposition was not observed. The trend of concentration profiles for individual elements in the boundary, documented in Figure 16, proves that all active elements contributed to bond formation, but in Figure 16d), an increased Mg concentration was observed in the boundary.

3.5. Microstructure of the Cu/Zn5Al3Mg Joint

The transition zone of the joint was primarily analyzed. In the Cu/Zn5Al3Mg joint boundary, two new intermetallic phases were observed, namely the $CuZn_4$-ε phase and a phase that, by the phase diagram in Figure 17, corresponds to the combination of the $Cu_{33}Al_{17}$ rt/Cu_9Al_4 rt/Cu_5Zn_8-γ phases. These phases are the result of Zn solder and copper substrate interaction. The $CuZn_4$-ε phase also occurs in the entire solder volume. Zn mainly contributes to bond formation, but the effect of Al upon bond formation was also observed. The effect of Mg on bond formation with the copper substrate is minimal.

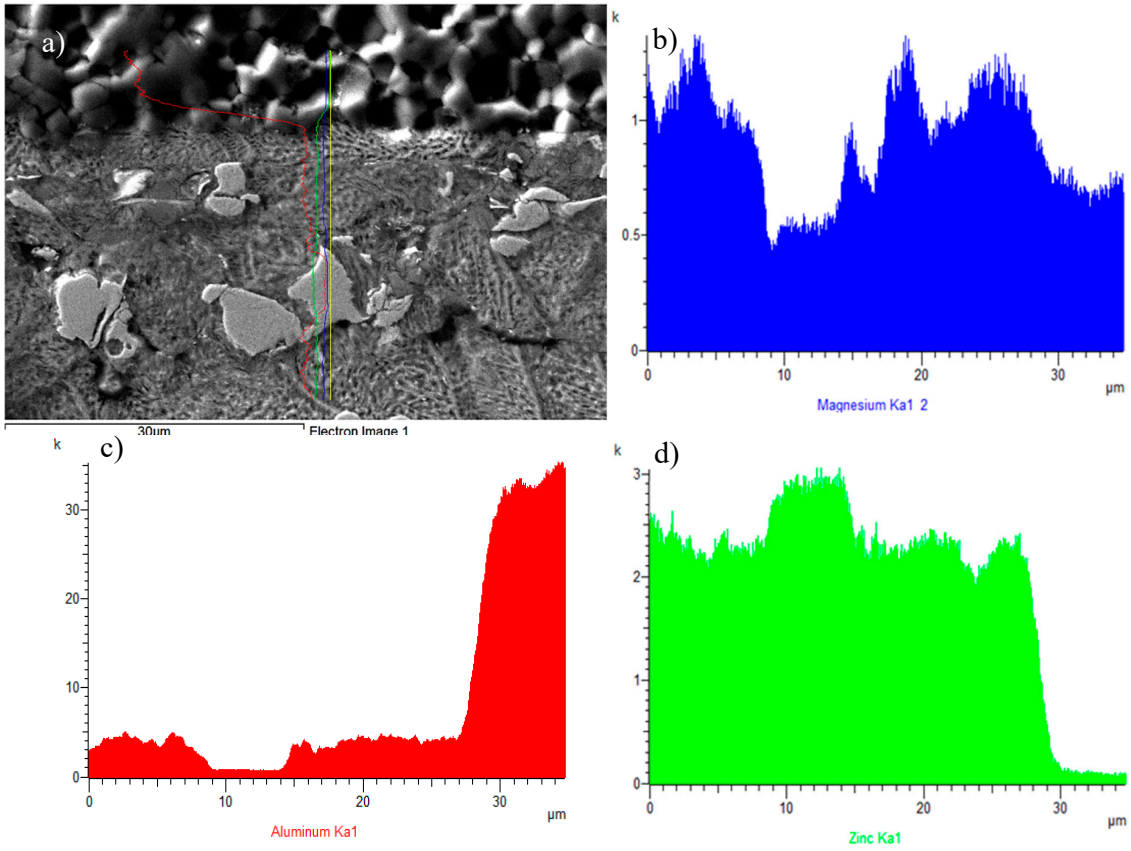

Figure 16. Concentration profiles of elements in the boundary of the AlN/Zn–Al–Mg joint, (**a**) joint microstructure, (**b**) Mg profile, (**c**) Al profile, (**d**) Zn profile.

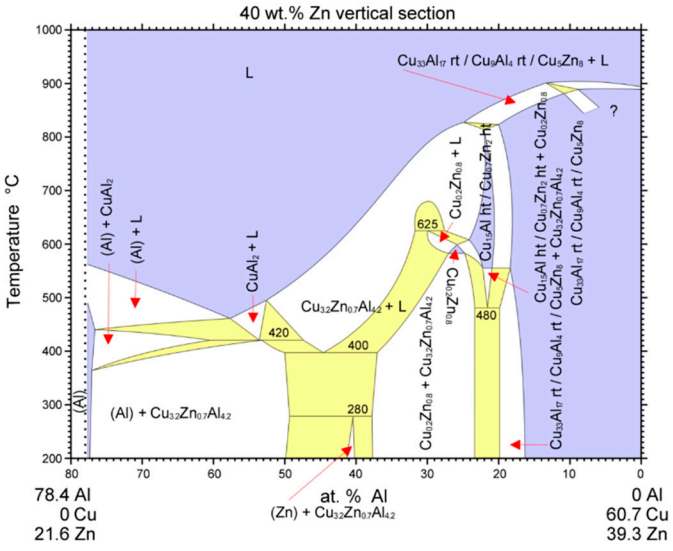

Figure 17. Isopletic section of ternary system Al-Cu for 40 wt % of Zn [22].

The $CuZn_4$ phase also occurs in the solder, and it contains a higher Zn content. It is wettable with the solder. In Figure 18 and Table 6, the $CuZn_4$ phase corresponds to the composition at point Spectrum 4, with the presence of approximately 2 wt % Al. Spectrum 3 is the $MgZn_2$ phase, where the presence of Al (2 wt %) and Cu (about 8 wt %), was observed.

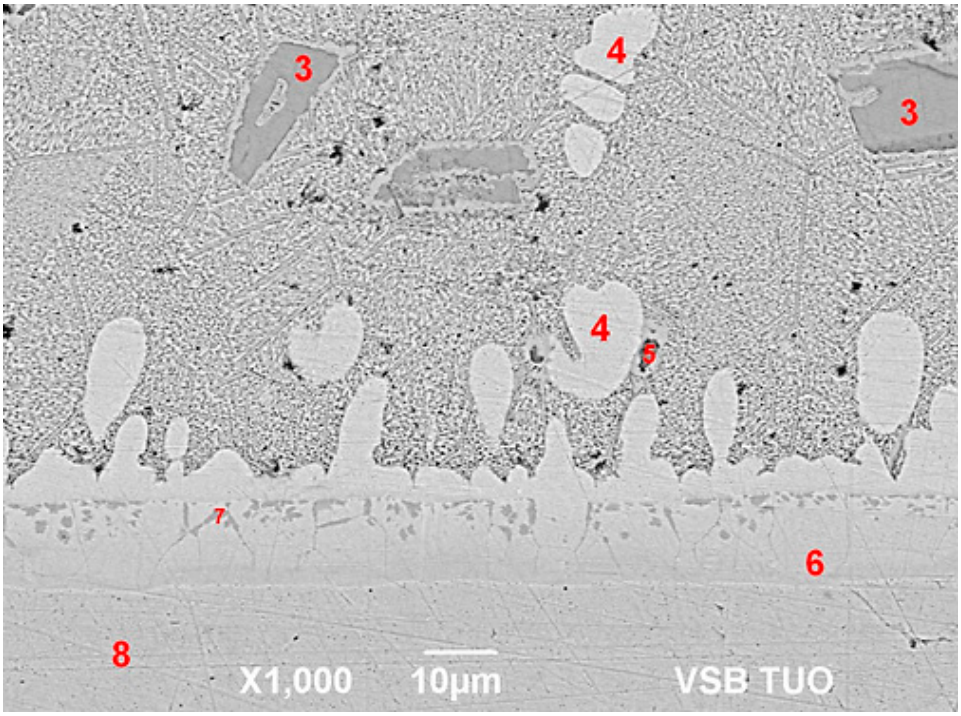

Figure 18. The EDX point analysis of the Cu/Zn5Al3Mg boundary.

Table 6. The phase composition results of Cu/Zn5Al3Mg boundary.

Spectrum	Zn [wt %]	Al [wt %]	Mg [wt %]	Cu [wt %]	Component
Spectrum 3	73.88	2.18	16.46	7.48	$MgZn_2$ phase
Spectrum 3	73.22	2.12	16.51	8.14	$MgZn_2$ phase
Spectrum 4	80.56	2.00	0	17.44	$CuZn_4$ phase
Spectrum 4	78.63	2.63	0	18.74	$CuZn_4$ phase
Spectrum 5	76.43	2.80	14.08	6.79	Probably $MgZn_2$ phase
Spectrum 6	39.71	8.38	0	51.91	Cu_5Zn_8 phase
Spectrum 6	42.10	7.77	0	50.13	Cu_5Zn_8 phase
Spectrum 7	33.41	13.26	0	53.53	-
Spectrum 7	33.84	13.21	0	52.96	-
Spectrum 8	0	0	0	100	pure Cu

The combined phase of $Cu_{33}Al_{17}$ rt/Cu_9Al_4 rt/Cu_5Zn_8-γ is closer to copper and, besides Zn, it also contains Al. In Figure 17, it corresponds to the composition at the point of measurement—Spectrum 6. Spectrum 7 contains a minority phase of $Cu_{33}Al1_7$ rt/Cu_9Al_4 rt/Cu_5Zn_8-γ, with high Al content.

The results of point EDX analysis are also proven by the trends in Zn, Al, Cu and Mg concentration profiles in Figure 19. Interestingly, the trend of Al concentration (light-blue color) is mainly in the new-formed zone with intermetallic phases. At first, no Al was observed in pure copper.

Then a gradual concentration increases in the first section of the transition zone, with Cu_5Zn_8 phases, was observed. Then the highest concentration of Al follows, in the zone with Cu–Al phases (dark-grey constituents). Subsequently, a reduced Al content in the second transition zone containing the $CuZn_4$ phase was observed.

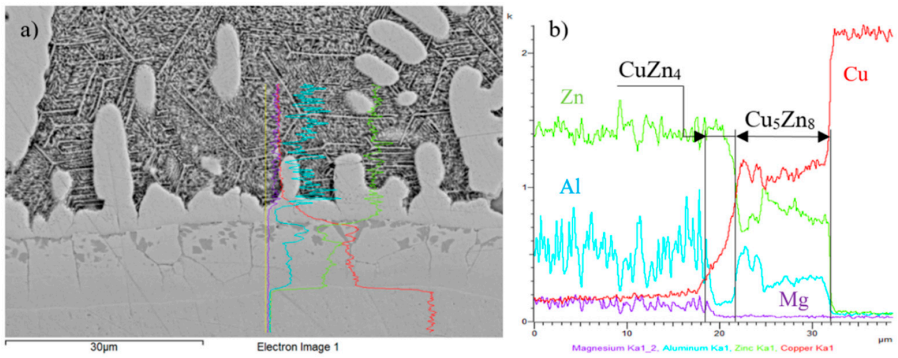

Figure 19. EDX analysis of the Cu/Zn5Al3Mg boundary; (**a**) microstructure of examined boundary; (**b**) concentration profiles of Zn, Cu, Al and Mg elements.

3.6. Shear Strength of Soldered Joints

The research in this study is primarily oriented to soldering AlN ceramics to a copper substrate. For results comparison, shear strength measurement was also performed on the Al_2O_3/Cu, SiC/Cu and Cu/Cu joints. The measurement was performed on three specimens of each material. The average shear strength results are documented in Figure 20.

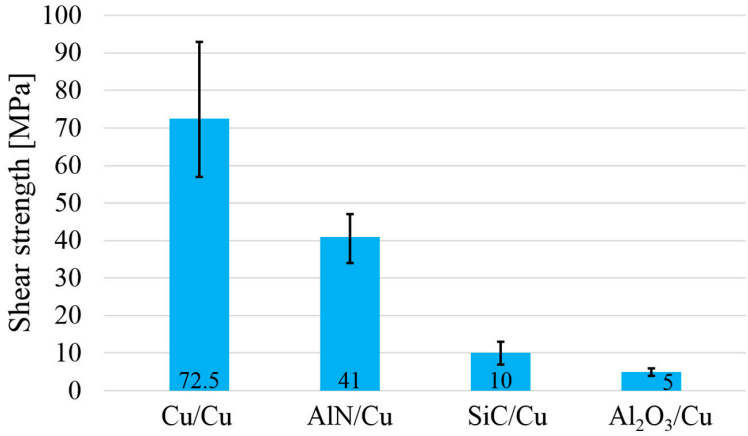

Figure 20. The shear strength of soldered joints.

The highest shear strength was achieved with the joint of two identical metals—Cu/Cu. The maximum shear strength of this joint was 93 MPa. In the case of the Cu shear strength measurement, it is necessary to take into account the formation of new intermetallic phases, such as $CuZn_4$ and Cu_5Zn_8, on the joint boundary. These phases increase the strength of the soldered joint. The highest shear strength in the combined ceramics/metal joints, namely 47 MPa, was observed in the AlN/Cu joint. It was just half of the shear strength of the Cu/Cu joint. This difference is caused by a different bond character on the ceramics/solder boundary. No new phase was formed in the ceramics/solder boundary. The mutual bond has an adhesive character. Therefore, low average values of shear strength, 10 and 5 MPa, were achieved with SiC/Cu and Al_2O_3/Cu joints, respectively.

For more precise identification, the fractured surfaces of joints were analyzed. Figure 21a,b show the fractured surfaces on the AlN/Zn5Al3Mg/Cu joint boundary. The fractured surface remained completely covered with solder. A ductile fracture occurred in the solder. An analysis of the planar distribution of Mg, Zn, Al and Cu elements was performed on the fractured surface, as documented in Figure 22b–e. In the fractured surface map, the Mg, Cu and Zn elements prevail. Therefore, the existence of the phases of those elements on the fractured surface may be supposed.

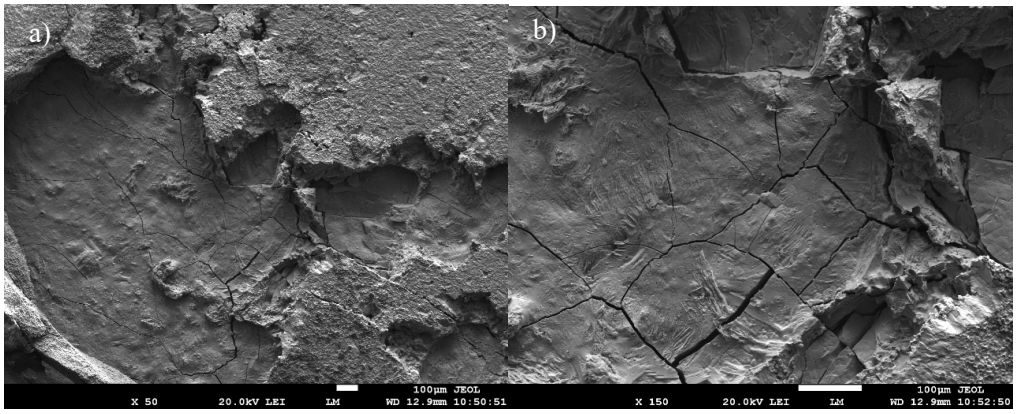

Figure 21. Fractured surface of soldered AlN/Zn5Al3Mg/Cu joint (**a**) magnification 50×, (**b**) magnification 150×.

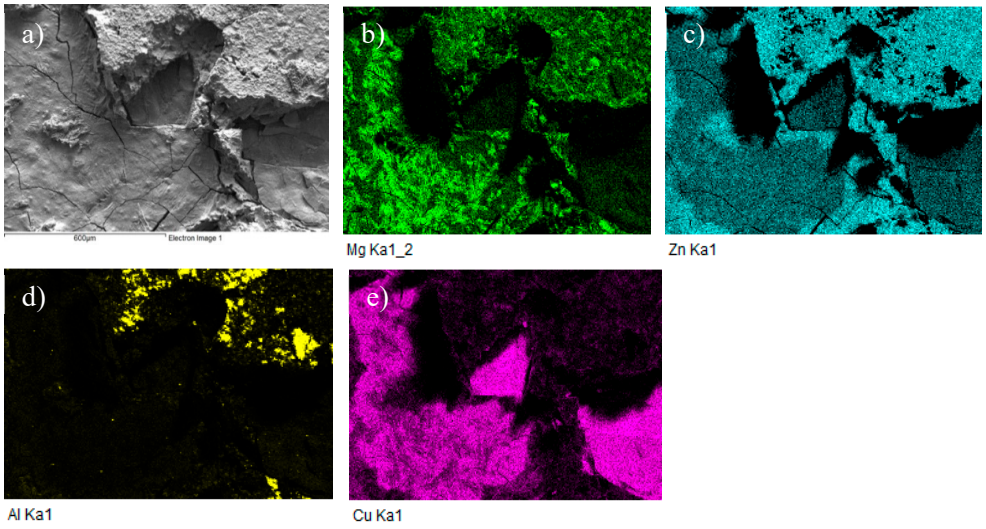

Figure 22. Fractured surface of soldered AlN/Zn5Al3Mg/Cu joint and the planar distribution of individual elements (**a**) fracture structure; (**b**) Mg; (**c**) Zn; (**d**) Al; (**e**) Cu.

From this viewpoint, an XRD analysis of the fractured surface of AlN/Zn5Al3Mg/Cu joint (Figure 23) was performed. The presence of AlN ceramics on the fractured surface was proven. Solid solutions of aluminum and zinc (Al), (Zn) and magnesium phases of Mg_2Zn_{11} and $MgZn_2$ were also observed. Additionally, new-developed phases of copper, namely, Cu_5Zn_8 and $CuAl_2$, were identified on the fractured surface, which are the result of solder interaction with the copper substrate. All these phases, except $CuAl_2$, were also proven by the EDX analysis.

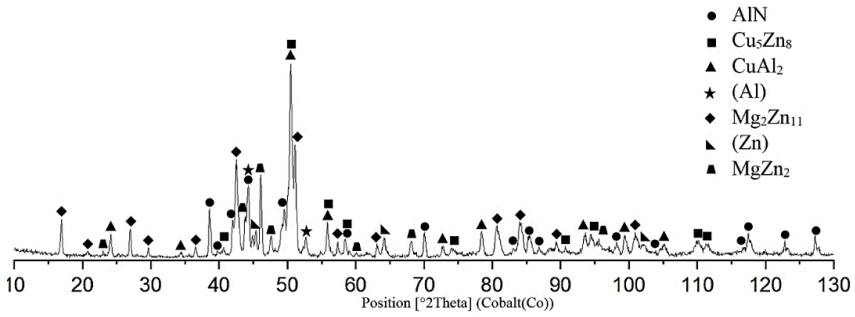

Figure 23. The XRD analysis of the fractured surface of AlN/Zn5Al3Mg/Cu joint.

4. Conclusions

The aim of this research consisted of analyzing Zn5Al-Mg soldering alloy. Whether the proposed composition of soldering alloy is suitable for soldering AlN ceramics and copper substrate at the defined conditions, was studied. To improve the wettability of ceramic material with Zn–Al–Mg solder, soldering with the assistance of active ultrasound was employed. The following results were achieved:

- DSC analysis was used for determining the solder melting point. The DSC curve contains two basic peaks with four thermal effects in the Al–Mg–Zn system. The first smaller peak corresponds to a eutectoid reaction with a 275 °C characteristic temperature. The second, larger peak corresponds to a eutectic reaction with a 340 °C characteristic temperature.
- The microstructure of Zn–Al–Mg solder is composed of solid solution (Al), solid solution (Zn) and Mg_2Zn_{11} phase, as was proven by XRD analysis. The EDX analysis has also revealed the minority $MgZn_2$ phase.
- The tensile strength of Zn–Al–Mg soldering alloys ranges from 82 to 169 MPa; the highest strength was observed in the solder with the lowest Mg content. Increasing Mg content in Zn–Al solder reduces the tensile strength, due to the formation of an Mg_2Zn_{11} phase, while the semi-quantitative analysis revealed 60% composition of this phase in the Zn5Al3Mg solder.
- The bond of AlN ceramics with the Zn5Al3Mg solder is formed as follows. Due to ultrasonic activation, the particles of zinc, aluminum and magnesium are distributed to the boundary with the ceramic substrate, while surface roughening and enhancing the solder wettability occurs. The EDX analysis has proven that all active elements, Al, Zn and Mg, contributed in the same manner to bond formation between AlN ceramics and this Zn–Al–Mg solder. No new transition phase was formed.
- The EDX analysis revealed two new intermetallic phases in the Cu/Zn5Al3Mg joint boundary, namely $CuZn_4$-ε and the phase that, according to the Al-Cu-Zn phase diagram, corresponds to a combination of $Cu_{33}Al_{17}$ rt/Cu_9Al_4 rt/Cu_5Zn_8-γ phases. These phases are the result of zinc solder and copper substrate interaction. The Cu_5Zn_8 phase was also proven by the XRD analysis of the fractured surface. The presence of a $CuAl_2$ phase was also identified by XDR analysis.
- The maximum shear strength of the combined AlN/Cu joints was 47 MPa. However, it is only half of the shear strength achieved with the Cu/Cu joint fabricated using the same solder type, Zn5Al3Mg. This difference is caused by the different character of bond formation in the ceramics/solder boundary. No new phase was formed in the ceramics/solder boundary and the mutual bond has an adhesive character.

Author Contributions: Supervision, R.K.; Investigation, I.K.; Formal analysis, J.D. and P.Z.; Data curation, M.K. All authors have read and agreed to the published version of the manuscript.

Funding: This research was funded by Slovak Research and Development Agency under contract no. APVV-17-0025; Slovak Scientific Grant Agency VEGA under contract no. VEGA 1/0303/20; and Project 1393 – Soldering - Excellent teams.

Acknowledgments: The paper was also prepared in cooperation with the VSB-Technical University of Ostrava, FMT-Faculty of Materials Science and Technology, Department of Non-ferrous Metals, Refining and Recycling.

Conflicts of Interest: The authors declare no conflict of interest.

References

1. Suganuma, K.; Kim, S.J.; Kim, K.S. High-Tepmerature Lead-Free Solders: Properties and Possibilities. *JOM* **2009**, *61*, 64–71. [CrossRef]
2. Chidambaram, V.; Hattel, J.; Hald, J. Design of lead-free candidate alloys for high-temperature soldering based on the Au–Sn system. *Mater. Des.* **2010**, *31*, 4638–4645. [CrossRef]
3. Watson, J.; Castro, G. High-Temperature Electronics Pose Design and Reliability Challenges. *Analog Dialogue* **2012**, *46*, 3–9.

4. Kim, J.H.; Jeong, S.W.; Lee, H.M. Thermodynamics aided alloy design and evaluation of Pb-free solders for high-temperature applications. *Mater. Trans.* **2002**, *43*, 1873–1878. [CrossRef]
5. Mician, M.; Konar, R. Repairs of damaged castings made of graphitic cast iron by means of brazing. *Arch. Foundry Eng.* **2017**, *17*, 91–96. [CrossRef]
6. Bobzin, K.; Schlafer, T.; Kopp, N. Thermochemistry of brazing ceramics and metals in air. *Int. J. Mater. Res.* **2011**, *102*, 972–976. [CrossRef]
7. Zhao, Y.X.; Wang, M.R.; Cao, J.; Song, X.G.; Tang, D.Y.; Feng, J.C. Brazing TC4 alloy to Si3N4 ceramic using nano-Si3N4 reinforced AgCu composite filler. *Mater. Des.* **2015**, *76*, 40–46. [CrossRef]
8. Hong, L.; Xuan, L.; Haixin, H. Microstructure and properties of ZrO_2 ceramic and Ti-6Al-4V alloy vacuum brazed by Ti-28Ni filler metal. *Weld. Technol. Rev.* **2019**, *91*, 35–41. [CrossRef]
9. Chidambaram, V.; Hald, J.; Hattel, J. Development of Au-Ge based candidate alloys as an alternative to high-lead content solders. *J. Alloys Compd.* **2010**, *490*, 170–179. [CrossRef]
10. Kroupa, A.; Andersson, D.; Hoo, N.; Pearce, J.; Watson, A.; Dinsdale, A.; Mucklejohn, S. Current Problems and Possible Solutions in High-Temperature Lead-Free Soldering. *J. Mater. Eng. Perform.* **2011**, *21*, 629–637. [CrossRef]
11. Rettenmayr, M.; Lambracht, P.; Kempf, B.; Graff, M. High melting Pb-free solder for die-attach applications. *J. Adv. Eng. Mater.* **2005**, *7*, 965–969. [CrossRef]
12. Hodúlová, E.; Li, H.; Šimeková, B.; Kovaříková, I. Structural analysis of SAC solder with Bi addition. *Weld. World* **2018**, *62*, 1311–1322. [CrossRef]
13. Cay, F.; Kurnaz, S.C. Hot tensile and fatigue of zinc-aluminium alloys produced by gravity and squeeze casting. *Mater. Des.* **2005**, *26*, 479–485. [CrossRef]
14. Haque, A.; Lim, B.H.; Haseeb, A.S.M.A.; Masjuki, H.H. Die attach properties of Zn-Al-Mg-Ga based high-temperature lead-free solder on Cu lead-frame. *J. Mater. Sci. Mater. Electron.* **2012**, *23*, 115–123. [CrossRef]
15. Rettenmayr, M.; Lambracht, P.; Kempf, B.; Tschudin, C. Zn-Al based alloys as Pb-free solders for die attach. *J. Electron. Mater.* **2002**, *31*, 278–285. [CrossRef]
16. Cheng, F.; Gao, F.; Wang, Y.; Wu, Y.; Ma, Z.; Yang, J. Sn addition on the tensile properties of high temperature Zn-4Al-3Mg solder alloys. *Microelectron. Reliab.* **2012**, *52*, 579–584. [CrossRef]
17. Shimizu, T.; Ishikawa, H.; Ohnuma, I.; Ishida, K. Zn-Al-Mg-Ga Alloys as Pb-Free Solder for Die-Attaching Use. *J. Electron. Mater.* **1999**, *28*, 1172–1175. [CrossRef]
18. Chen, X.; Yan, J.; Ren, S.; Wang, Q.; Wei, J.; Fan, G. Microstructure, mechanical properties, and bonding mechanism of ultrasonic-assisted brazed joints of SiC ceramics with ZnAlMg filler metals in air. *Ceram. Int.* **2014**, *40*, 683–689. [CrossRef]
19. Cui, W.; Yan, J.; Dai, Y.; Li, D. Building a nano-crystalline α-alumina layer at a liquid metal/sapphire interface by ultrasound. *Ultrason. Sonochem.* **2015**, *22*, 108–112. [CrossRef]
20. Cui, W.; Li, S.; Yan, J.; Zhang, X. Microstructure and mechanical performance of composite joints of sapphire by ultrasonic-assisted brazing. *J. Mater. Process. Technol.* **2018**, *257*, 1–6. [CrossRef]
21. *Binary Alloy Phase Diagrams*; ASM International: Materials Park, OH, USA, 2000.
22. Kartavykh, A.V.; Tcherdyntsev, V.V.; Zollinger, J. TiAl–Nb melt interaction with AlN refractory crucibles. *Mater. Chem. Phys.* **2009**, *116*, 300–304. [CrossRef]